

# Training Frankenstein’s Creature to Stack: HyperTree Architecture Search

Andrew Hundt<sup>1</sup>, Varun Jain<sup>1</sup>, Chris Paxton<sup>2</sup>, Gregory D. Hager<sup>1</sup>

**Abstract**— We propose HyperTrees for the low cost automatic design of multiple-input neural network models. Much like how Dr. Frankenstein’s creature was assembled from pieces before he came to life in the eponymous book, HyperTrees combine parts of other architectures to optimize for a new problem domain. We compare HyperTrees to rENAS, our extension of Efficient Neural Architecture Search (ENAS) [1]. To evaluate these architectures we introduce the CoSTAR Block Stacking Dataset for the benchmarking of neural network models. We utilize 5.1 cm colored blocks and introduce complexity with a stacking task, a bin providing wall obstacles, dramatic lighting variation, and object ambiguity in the depth space. We demonstrate HyperTrees and rENAS on this dataset by predicting full 3D poses semantically for the purpose of grasping and placing specific objects. Inputs to the network include RGB images, the current gripper pose, and the action to take. Predictions with our best model are accurate to within 30 degrees 90% of the time, 4cm 72% of the time, and have an average test error of 3.3cm and 12.6 degrees. The dataset contains more than 10,000 stacking attempts and 1 million frames of real data. Code and dataset instructions are available at [github.com/jhu-lcsr/costar\\_plan](https://github.com/jhu-lcsr/costar_plan).

## I. INTRODUCTION

The recent success of deep learning (DL) on challenging computer vision tasks has spurred efforts to develop DL systems that can be applied to perception-based robotics [3], [4]. The promise of DL is that it might be possible to train a system, from representative data, to solve complex, perception-based robotics tasks in realistic environments with higher reliability and less programming effort than traditional programming methods. However, the reality is that progress in this area faces two fundamental challenges. First, representative data from complete real-world robotics tasks is limited and difficult to structure, hindering the development and benchmarking of new algorithms. Second, the process of designing and training a DL architecture is itself a time consuming, complicated, highly empirical process [3], [5], [6]. This is especially true in robotics, where multiple types of sensor data including arm position and camera images might need to be integrated.

In this paper, we address both of these issues. First, we introduce the CoSTAR Block Stacking Dataset. Currently available data sets for robotic manipulation include [3], [7], [8], [9]. These data sets provide good representation of certain aspects of manipulation, but don’t incorporate a complete end-to-end task. Furthermore, common sources of real-world variation are reduced by limiting the workspace

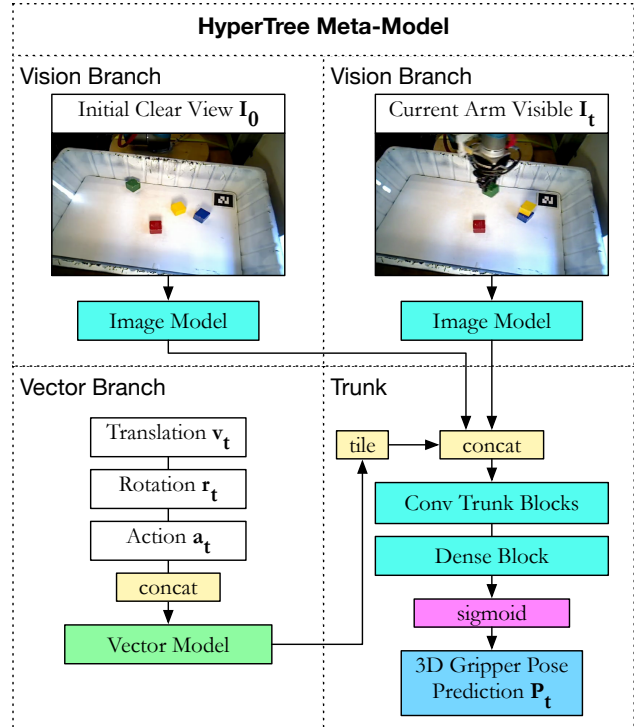


Fig. 1: A detailed view of the HyperTree MetaModel configured for predicting 3D ground truth goal poses,  $G_t$ , on the block stacking dataset. HyperTrees can accept an arbitrary number of image and vector inputs. Hyperparameter definitions are in Table II. Details for the dataset are in Fig. 2, 3, and Table I. Supplementary video is at [sites.google.com/view/hypertree-renas](https://sites.google.com/view/hypertree-renas).

to one without obstacles[3], [5], omitting sunlight [10], and limiting surrounding scenes [10], [11]. We designed the CoSTAR Block Stacking Dataset as a benchmark for performing complex, multi-step manipulation tasks in challenging scenes. In this dataset, a robot attempts to stack 3 simple colored blocks in a specific order to explore deep learning for robotic manipulation with simple target objects in a cluttered and variable surrounding environment. The dataset includes subsets with and without distractors.

As noted above, robotic neural network architectures and their hyperparameters are still regularly handmade for new tasks [3], [5], [4], and automatic design can be expensive [6]. One solution might be simulation to real transfer, but that itself remains an open problem. Another possibility is neural network architecture search, which is a challenging problem

<sup>1</sup> Johns Hopkins University Department of Computer Science. {ahundt, jain, cpaxton, ghager1}@jhu.edu

<sup>2</sup> Chris Paxton is with NVIDIA, Seattle WA 98105



Fig. 2: The CoSTAR system [2] collecting the block stacking dataset. Each example consists of an attempt to stack 3 colored blocks in a specified order.

even in domains that do not need to integrate multiple types of information. For example, NASNet [6] employed 450 GPUs for 3-4 days (32k-43k GPU-hours) to design an architecture for image classification tasks. Recent work has attempted to reduce the number of GPU-hours needed for automatic neural network architecture design, and Efficient Neural Architecture Search (ENAS) [1] can now achieve results competitive with NASNet using just 16 GPU-hours of processing. This suggests that developing new automated architecture search methods specific to robotics may offer a path toward more efficient development of DL architectures.

To summarize, we make the following contributions:

- 1) HyperTree Architecture search for low cost automatic design of neural network models which require multiple input data streams.
- 2) rENAS, an extension of Efficient Neural Architecture Search (ENAS) [1] to regression and multi-input data streams.
- 3) An approach to semantic action planning which generates full 3D gripper pose proposals for both object grasping and placement.
- 4) The publicly-available CoSTAR Block Stacking Dataset, which provides over 10,000 annotated real robot trials.

We also analyze the performance of the best neural network architectures chosen by HyperTree search and rENAS on the CoSTAR Block Stacking Dataset.

## II. RELATED WORK

Recent advances in deep learning have revolutionized robotic grasping with perception based methods learned from big data [3], [4], [11], [12], [13], [14], [15]. Other work has investigated learning from simulation and then incorporating those models into robotic control [16]. Others have used reinforcement learning for generating API calls for pre-programmed actions [17].

One notable limitation of past approaches to robotic manipulation is the restriction of end effector poses to be

CoSTAR Block Stacking Dataset Summary		
<b>Calibrated images</b>	color, depth	
<b>Joint data</b>	angle, velocity	
<b>Labels</b>	action, success/failure/error.failure	
<b>Blocks</b>	red, green, yellow, blue	
<b>Block Actions</b>	grasp(block), place(block, on_block(s))	
<b>Location Action</b>	move_to(home)	
<b>Typical Timeline</b>	20s duration, 200 frames, 10Hz	
3D coordinate poses recorded		
gripper base and center	rgb camera	depth camera
robot joints	AR tags + ID#	colored blocks
	<b>blocks</b>	<b>blocks + toys</b>
Attempts	5,870	6,107
Successes	2,451	748
Failures, all kinds	3,419	5,359
Failures without errors	1228	3629
Failures with errors	2,191	1,730
<b>Success Only Subset</b>		
Training	2,195	620
Validation	128	64
Test	128	64

TABLE I: Summary of data available in the CoSTAR block stacking dataset shown in Fig. 2. Stacking was conducted under 2 conditions: (1) blocks only and (2) blocks with plush toy distractors. Failures with no errors complete 5 actions but are unsuccessful at stacking. Causes of failures with errors include security stops from collisions, user emergency stops, planning failures, and software runtime errors.

either vertical and facing down or normal to local depth values, with only an angular parameter available to define orientation changes [3], [4], [5], [18]. Also common is the use of depth-only data [4] which precludes the possibility of object discrimination based on color. Furthermore, such analysis may have been performed in lighting conditions that are very consistent, which can lead to failures in the presence of direct sunlight. Progress towards semantic grasping of specific objects [19] is substantial, but it remains an open problem.

Finally, automatic model design is an emerging way to define neural networks, but a broad overview is outside the scope of this paper so we refer to a recent survey [20].

## III. BLOCK STACKING DATASET

We define a block stacking task where a robot attempts to stack 3 of 4 colored blocks in a specified order. The robot can be seen in Fig. 2, and examples of key image frames for two successful stack attempts are shown in Fig. 3. A dataset summary can be found in Table I, and it includes subsets with and without plush toy distractors.

Data is collected utilizing our prior work on the collaborative manipulation system CoSTAR [2] and our recent work on motion and task planning [21]. CoSTAR is a system designed for end-user creation of robot task plans that offers a range of capabilities plus a rudimentary perception system based on ObjRecRANSAC [2], [22]. In a single stack attempt the robot aims to complete a stack by performing 5 actions: 2 repetitions of the CoSTAR SmartGrasp and SmartPlace actions, plus a final move to the home position above the bin. The sequence pictured in the first

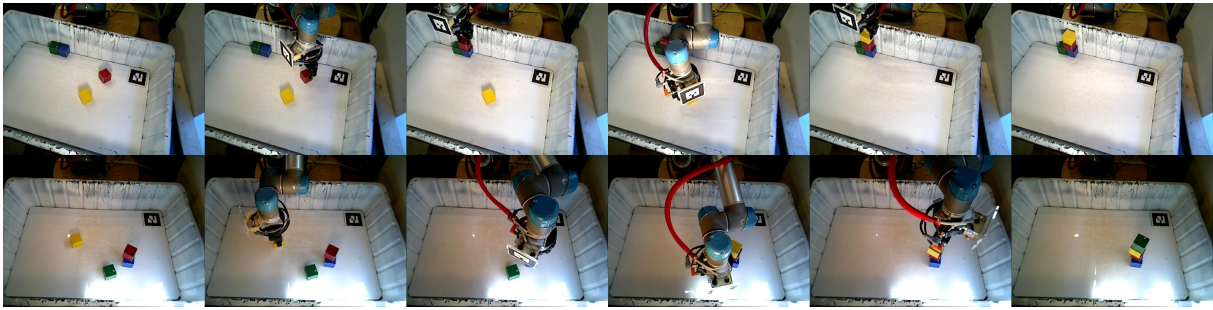


Fig. 3: Each row demonstrates a separate successful block stacking attempt. A sequence starts on the left with a clear view at frame  $I_0$  then proceeds right showing the timesteps of the 5 goal poses  $G_t$  (Eq. 2, and Fig. 2) at which the gripper may open or close. Notice the variation in bin position, gripper tilt, the challenging lighting conditions, the stack of 4 blocks, and the object wear. Viewing video and other details is highly recommended, see [sites.google.com/site/costardataset](https://sites.google.com/site/costardataset).

row of in Fig. 3 consists of the following 5 actions from left to right: `grasp(red)`, `place(red, on.blue)`, `grasp(yellow)`, `place(yellow, on.red.blue)`, and `move(home)`. There are a total of 41 possible actions: grasp actions interact with each of the 4 colored blocks (4 actions), placement actions are defined for ordered stacks with up to height 2 (36 actions). These combined with the `move(home)` action add up to a total of 41 possible actions.

The dataset provides the appearance of smooth actions with the gripper entering the frame, creating a stack in the scene, and finally exiting the frame at the end. During real time execution the robot (1) proceeds to a goal, (2) saves the current robot pose, (3) stops recording data, (4) moves out of camera view to the home position, (5) estimates the block poses, (6) moves back to the saved pose, (7) resumes recording, (8) starts the next action. After moving to the final home position object poses are estimated and the maximum  $z$  height of a block determines stack success which is confirmed with human labeling. Some features, such as collision checks, are disabled so that a set of near-collision successes and failures may be recorded.

#### IV. PROBLEM AND APPROACH

We begin by distinguishing between one-shot pose estimation problems and tasks such as object grasping and placement. Pose estimation is typically a one timestep prediction [23], [24]. Grasping and placement are actions that run continuously and which might be refined multiple times as the gripper approaches a goal. This makes it possible for grasping to be robust to hand eye calibration changes and missed grasps in a way that a one time pose estimate cannot [3], [5]. We illustrate the refinement of a goal pose as a goal is approached qualitatively in our supplementary video.

##### A. Goals and Encodings

Each successful stacking attempt consists of 5 separate actions out of 41 possible actions as illustrated in Fig. 3. Predictions  $P_t$  are made with respect to ground truth goal poses  $G_t$  at the end of each action. Stacking attempts and individual actions vary in duration and both are divided into

separate 100 ms time steps  $t$  out of a total  $T$ . There is also a pose consisting of translation  $v$  and rotation  $r$  at each time step (2), which are encoded between [0,1] for use in a neural network as follows: The **translation vector encoding** is  $v = (x, y, z)/d + 0.5$ , where  $d$  is the maximum workspace diameter in meters. The **Rotation  $r$  axis-angle encoding** is  $r = (a_x, a_y, a_z, \sin(\theta), \cos(\theta))/s + 0.5$ , where  $a_x, a_y, a_z$  is the axis vector for gripper rotation,  $\theta$  is the angle to rotate gripper in radians, and  $s$  is a weighting factor relative to translation. **Example  $E$  is the input to the neural network:**

$$E_t = (I_0, I_t, v_t, r_t, a_t) \quad (1)$$

Where  $I_0$  and  $I_t$  are the initial and current images,  $v_t, r_t$  are the respective base to gripper translation and rotation (Fig. 2).  $a_t$  is the action one-hot encoding of 41 actions. **Ground Truth Goal Pose  $G_t$**  from Fig. 2 is the 3D pose at time  $g$  at which the gripper trigger to open or close, ending an action in a successful stacking attempt:

$$G_t = (v_t^g, r_t^g) | t \leq g \leq T, e_g \neq e_{g-1}, a_g == a_t \quad (2)$$

where  $g$  is the first time the gripper moves after  $t$ ,  $e$  is the gripper open/closed position in [0, 1]. The goal is defined by when the gripper position changes. In what follows,  $P_t = (v_t^p, r_t^p)$  is a prediction of  $G_t$ .

Each example  $E_t$  has a separate sub-goal  $G_t$  defined by (1) the current action  $a_t$  and (2) the robot's 3D gripper pose relative to the robot base frame at the time step  $g$  when the gripper begins moving to either grasp or release an object. Motion of the gripper also signals the end of the current action, excluding the final `move(home)` action, which has a fixed goal pose.

##### B. HyperTree MetaModel

We have noticed that many robotics papers utilizing deep neural network architectures share common architecture elements [3], [4], [25]. Broadly, each has inputs for images and/or vectors which are each processed by some number of neural network layers, though the structure varies. These components may then be concatenated to apply additional blocks of layers for data fusion. The output of these layers are subsequently split to one or more block sequences, typically

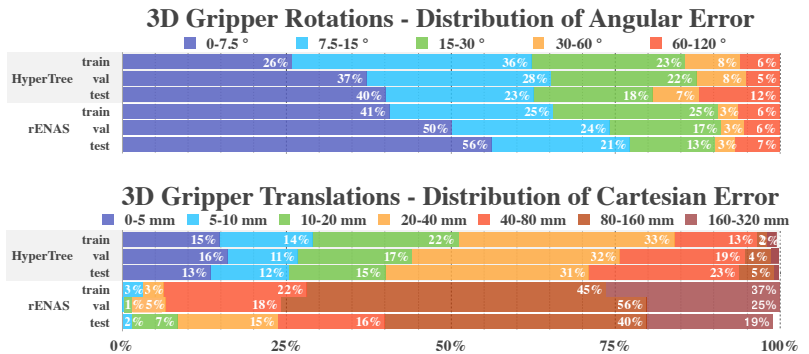
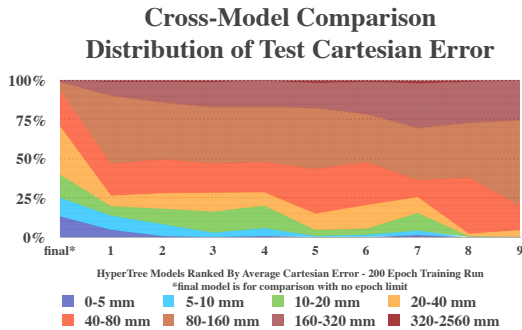


Fig. 4: **(All)** The best models’ predictions  $P_t$  against ground truth  $G_t$  at random times  $t$ . A high percentage of samples with low error is better. **(Left)** The importance of hyperparameter choice is visible in models 1-9 which were selected from the best of 1100 HyperTree candidates and then trained for 200 epochs. **(Top)** Distribution of angular error between predicted and actual 3D gripper rotations  $\Delta Rot(r_t^p, r_t^g)$  (Eq. 2, and Fig. 2). **(Bottom)** Distribution of translation error  $\|v_t^p - v_t^g\|$  (Eq. 2, and Fig. 2).

dense layers. Finally, in the case of vector outputs there may be a pooling operation followed by activation, or the latent variables may simply be activated at each location in the case of pixel-wise outputs. Architectures fitting this layout have been partially or fully designed by hand in a completely reasonable manner, but is each the optimal choice for that domain? To investigate this question we designed the HyperTree MetaModel (Fig. 1) and parameterized it (Table II) so that models and their constituent parts might be defined, swapped, evaluated and optimized in a fully automatic fashion. In fact, a HyperTree MetaModel’s search space can be defined to generalize many of the previously referenced architectures as a special case.

### C. HyperTree Architecture Search

We define a HyperTree network using Keras [26] backed by Tensorflow [27] in search of a model which can most accurately predict the solution to a specific problem. We explore and then optimize the models’ hyperparameter network structure using GPyOpt [28]. HyperTree search repeatedly runs a sampling from 100 random architectures and then estimates 10 additional random architectures by optimizing the Expected Improvement (EI) in training loss with a predictive Sparse Gaussian Process Model (SGPM). These limits were chosen due to the practical tradeoff between processing time and memory utilization when evaluating the SGPM, since we found GPyOpt prediction time outstripped model evaluation time with large sample sizes.

In practice, we (1) run HyperTree search for 1 epoch on between 500-5,000 models with augmentation disabled depending on the available computing resources and dataset size. From this we (2) automatically construct a table of the best models, which we sort by a chosen metric, typically the average cartesian or angular validation error. We then (3) conduct a second automated training run proceeding down the top 1-10% of this sorted list for 10 epochs per model, which is added to our model table. In step (4) we repeat steps 2 and 3 for 200 epochs with 2-10 models and augmentation enabled, if appropriate. Step (5) is a 600 epoch training run

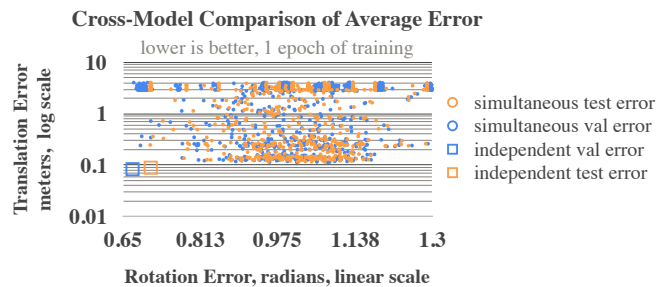


Fig. 5: A cross-model comparison of average error with 1 epoch of training. Each dot represents a single HyperTree architecture which predicts both translation and orientation,  $P_t$ . The squares demonstrate how a selected pair of HyperTree architectures reduce error by predicting translation  $v_t^p$  and rotation  $r_t^p$  independently.

initialized with the best model from step 4 resumed as needed until convergence, to reach a final model according to the chosen validation metric. An optional step (6) is to manually narrow the hyperparameter search space to ranges defined by the best image and trunk models and repeat steps 1-5.

Variables, dimensions and inputs above (as in Sec. IV-A and IV-B) are parameterized. For example, HyperTrees accept zero or more vector and image inputs. The Cornell Grasping Dataset provides one image, and we utilize two on the block stacking dataset. Block stacking results are described in Fig. 4, Table II, and Section V.

### D. Regression ENAS

A complementary approach to HyperTree search is ENAS [1], which trains an LSTM with a policy gradient in search of an optimal subgraph within a large graph representing possible architectures. We investigated ENAS to determine how effective its search paradigm is in comparison to HyperTrees. We were able to generate similar results on CIFAR-10 [35] and confirmed the approach by adapting their work for training on the **Fashion-MNIST dataset** [36] with which we found a state of the art micro-search architecture with 99.2% validation accuracy.

Hyperparameter	Search Space	Translation Model	Rotation Model
Image Model	[VGG, DN, RN, IRNv2, NAS]	NAS	VGG16
Trainable Image Model Weights*	[True, False]	True	True
CoordConv Layer Location	[None, Pre-Trunk, Pre-Image]	None	Pre-Trunk
Loss Function*	[mse, mae, msle]	mse	msle
Activation (Conv3x3, Vector Block, Dense Block)	[relu, elu, linear]	relu, relu, relu	N/A, relu, relu
Vector Block Model	[Dense, DN]	Dense	DN
Vector Block Layer Count	$n \in [0..5)$	2	1
Conv Trunk Block Model	[Conv3x3, NAS, DN, RN]	Conv3x3	NAS
Conv Trunk Block Count	$n \in [0..11)$	8	8
Filters (Vector, Trunk, Dense Block)	$2^n   n \in [6..13), [6..12), [6..14)$	2048, 1024, 512	256, 32, 2048
Dense Block Layer Count	$n \in [0..5)$	2	3
Normalization (Vector, Trunk)	[Batch, Group, None]	Batch, None	Batch, Batch
Optimizer*	[SGD, Adam]	SGD	SGD
Initial Learning Rate*	$0.9^n   n \in [0.0..100.0]$ continuous	1.0	1.0
Dropout rate*	[0, 1/8, 1/5, 1/4, 1/2, 3/4]	1/5	1/5

TABLE II: Architecture Search Parameters for the HyperTree MetaModel defined in Figure 1. Image Models: VGG16 [29], DN is DenseNet 121 [30], RN is ResNet 50 [31], [32], IRNv2 is Inception ResNetv2 [33], NAS is NASNet Mobile [6]. For network blocks, NAS refers to the "NASNet A Cell", DN refers to the DenseNet Dense Block, and ResNet refers to their Identity Block. The Activation hyperparameter applies to the Vector Model, the Conv3x3 Trunk Block, and the Dense Layers in the Dense Block. CoordConv [34] "Pre-Image" applies an initial CoordConv Layer to each input image and CoordConv Pre-Trunk applies a CoordConv layer after the vision and vector branches have been concatenated in the HyperTree Trunk. In the Vector Block "Dense" is a sequence of Dense Layers, while "DNBlock" is a DenseNet style block where Dense layers replace convolutions for the purpose of working with 1D input. Starred \* parameters were searched then locked in manually for subsequent searches to ensure consistency across models.

For the CoSTAR Block stacking dataset we adapt the original ENAS to accept arbitrary 3D tensors, replace all fixed average pooling layers with max pooling layers, and enable a final sigmoid activation in place of softmax for the regression of positions and orientations. To suit this new problem class we increase number of cells (Fig. 6) and parameterize the distance between each reduction cell to be every 2 cells, increasing the receptive field size to support larger images. We also reduced the number of blocks within a cell to 3. The vector input is tiled and then the initial image, current image, and tiled input vector are directly concatenated then fed to ENAS. In other words, the channels for a single pixel in the rotation case are (rgb, rgb,  $a_t$ ,  $v_t$ ,  $r_t$ ).

Our translation loss is Mean Squared Error (MSE) or  $L(m; \omega) = \frac{1}{N} \sum_{i=1}^N (x_i - y_i)^2$ , and the rotation loss is Mean Squared Logarithmic Error (MSLE)  $L(m; \omega) = \frac{1}{N} \sum_{i=1}^N (\log(x_i) - \log(y_i))^2$  computed on a batch of example data (Eq. 1) while keeping the controller policy fixed.

The gradient for a child model of rENAS and ENAS before it are defined as follows, with variable definitions below:

$$\nabla_{\omega} \mathbb{E}_{m \sim \pi(m; \Theta)} [L(m; \omega)] \approx \frac{1}{M} \sum_{i=1}^M \nabla_{\omega} L(m_i; \omega) \quad (3)$$

where  $\Theta$  is parameters of the controller LSTM,  $\omega$  is the parameters of the child model,  $\pi(m; \Theta)$  is the fixed controller policy, and  $m$  is a model sampled from the controller policy. During controller training, we fix  $\omega$  and update  $\Theta$ , aiming to maximize the expected reward  $\mathbb{E}_{m \sim \pi(m; \Theta)} R(m, \omega)$ . The

reward is computed on the validation set for training gripper rotations and translations as follows:

$$R(m, \omega) = \frac{1}{\max(|L(m; \omega)|, \epsilon)} \quad (4)$$

where  $\epsilon = 10^{-12}$ , a small nonzero value. We find this new function to be a reasonable metric when searching neural architectures for regression problems, as the reward will double whenever the loss halves, except in the case of 0 loss. Both ENAS and rENAS architecture search occur entirely in GPU memory, so searches take substantially more memory than HyperTrees, necessitating small 64x64 images. Our final two rotation cell architectures are in Fig. 6. Results are described in Fig. 4, and Section V. The code for our experiments on rENAS is available at [github.com/ahundt/enas](https://github.com/ahundt/enas).

## V. RESULTS

**Cornell Grasping Dataset:** To first confirm the generality of HyperTree search we applied it to the Cornell Grasping Dataset [7] and generated a model with 96% classification accuracy on object-wise 5-fold cross evaluation, compared with 93% for DexNet 2.0 [4].

**Separation of translation and rotation models:** In our initial search of the CoSTAR Block Stacking Dataset, a single model contained a final dense layer which output 8 sigmoid values encoding  $P_t$ . The results of this search represent 1,229 models which are pictured as dots in Fig. 5. The figure demonstrates that we found no models which were effective for both translation  $v_t^p$  and rotation  $r_t^p$  simultaneously. This observation led us to conduct independent

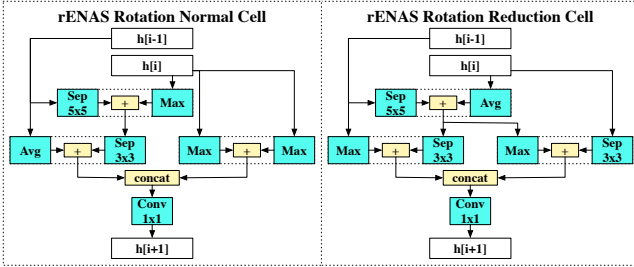


Fig. 6: Final rENAS micro-search rotation cells.

model searches with one producing 3 sigmoid values  $v_t^D$  (Eq. 2) encoding translations, and 5 sigmoid values predicting  $r_t^D$  (Eq.2) encoding rotations in  $P_t$  (Eq. 2). You can see an example of the resulting improvement in performance plotted as squares in Fig. 5.

**CoSTAR Block Stacking Dataset:** The hyperparameters of the best models resulting from the separate translation and rotation model searches are in Table II, while the performance of the top translation and rotation model is detailed in Fig. 4 for the training, validation, and test data. Results are presented on the success-only non-plush subset because the plush subset was being prepared at the time of writing. For translations on the HyperTree network, 67% of test pose predictions are within 4 cm and the average error is 3.3 cm. rENAS translations did not perform as well with 24% of test predictions within 4 cm and an average error of 12 cm. For comparison, the colored blocks are 5.1 cm on a side. 77% of rENAS rotation test prediction are within  $15^\circ$  of error, and the average rotation error is  $12.6^\circ$ . HyperTrees have 62% of rotation predictions within  $15^\circ$  and an average test angular error of  $18.3^\circ$ .

We suspect that rENAS translation performance may be limited by several factors. Specifically, ENAS itself was designed with fixed hyperparameters such as the number of filters in layers, the number of cells, the number of blocks in a cell, and so on. A more extensive automated search of ENAS hyperparameters may be necessary for certain problem types, though this might have a substantial impact on the GPU time required to find a high quality model.

**GPU Time:** HyperTree model search takes approximately 3k GPU-hours on the CoSTAR Block stacking dataset with 3 GPUs: 1 Titan X, 1 GTX 1080 Ti, and 1 GTX 1080 GPU. rENAS model search takes approximately 20 GPU-hours on a GTX 1080 Ti, depending on model size, and training takes approximately 22 hours, for a total of 42 GPU Hours. We note that rENAS (and ENAS before it) fixes many hyperparameters which were manually tuned, and HyperTrees outperforms rENAS for cartesian models.

#### A. Ablation Study

In essence, HyperTree search is itself an automated ablation study on the usefulness of each component in its own structure. This is because the HyperTree search space directly covers the cases where the Vector Model, Trunk Model, Dense Block, CoordConv Trunk, and CoordConv Image layers are removed. Specifically, a particular component is

skipped when the number of layers in Table II corresponding to that component has a value of 0 or None. For this reason, the best HyperTree models will either have or lack these components depending solely on the ranking of validation performance (Fig. 5), which is subsequently confirmed based on performance on the test data.

An additional HyperTree search of 1100 cartesian models confirms that differences in model quality persist with additional training (Fig. 4). This search specified a NASNet-Mobile [6] image model and either a Conv3x3 or NASNet model A cell trunk, selected to explore the space around our final cartesian model. We conducted an initial 1 epoch run, a second 40 epoch run, and then a final 200 epoch run on the 9 best models with respect to validation cartesian error. The hyperparameters of the top 9 models vary widely within the search space. Examples variation include: 0-3 vector branch layers, both vector block models, 0-4 dense block layers, 2-10 trunk layers, 512-8192 vector filters, all 3 CoordConv options, and both trunk options.

The variety of effectiveness across models shown in Fig. 4 and 5 causes us to suspect that trivial hand selection of models might easily lead to incorrect broader conclusions about one particular approach to neural networks being ineffective, when it actually reflects poor hyperparameter choices. This may be an interesting topic of investigation in future research. Indeed, we found the selection of 8 separate 32 filter NasNet A cells in our own best rotation HyperTree model (Table II) to be very surprising, and it is an option we would be unlikely to select by hand.

## VI. CONCLUSION

In conclusion, the automatic design of neural networks is an important step we believe will be necessary for broad and diverse deployment in robotics applications. Our contributions include two approaches for the low cost automatic design of neural networks with multiple inputs: HyperTree Architecture Search and rENAS. We have demonstrated the importance of hyperparameter choice via ablation studies, and demonstrate architecture search methods across multiple datasets including the CoSTAR Block Stacking Dataset, the Cornell Grasping Dataset, and the Fashion-MNIST image classification dataset. We have introduced an approach to full 3D object grasp and placement proposals which do not require object models, making it possible to grasp objects from one orientation to place in another for the purpose of completing a specific task. The GPU resources required by both rENAS and HyperTrees are within the reach of a single deep learning workstation, so they represent an effective approach to low cost automatic design of neural network models with a unique multi-input capability.

## VII. ACKNOWLEDGEMENTS

We thank Chunting Jiao and Chia-Hung Lin for their assistance with data collection and processing. This material is based upon work supported by the National Science Foundation under NRI Grant Award No. 1637949.

## REFERENCES

- [1] H. Pham, M. Y. Guan, B. Zoph, Q. V. Le, and J. Dean, "Efficient neural architecture search via parameters sharing," *International Conference on Machine Learning*, pp. 4092–4101, 2018. [Online]. Available: <http://arxiv.org/abs/1802.03268>
- [2] C. Paxton, A. Hundt, F. Jonathan, K. Guerin, and G. D. Hager, "CoSTAR: Instructing collaborative robots with behavior trees and vision," *Robotics and Automation (ICRA), 2017 IEEE International Conference on*, 2017. [Online]. Available: <https://arxiv.org/abs/1611.06145>
- [3] S. Levine, P. Pastor, A. Krizhevsky, J. Ibarz, and D. Quillen, "Learning hand-eye coordination for robotic grasping with deep learning and large-scale data collection," *The International Journal of Robotics Research*, vol. 37, no. 4-5, pp. 421–436, 2018, dataset:<https://sites.google.com/site/brainrobotdata/home>. [Online]. Available: <https://doi.org/10.1177/0278364917710318>
- [4] J. Mahler, J. Liang, S. Niyaz, M. Laskey, R. Doan, X. Liu, J. A. Ojea, and K. Goldberg, "Dex-net 2.0: Deep learning to plan robust grasps with synthetic point clouds and analytic grasp metrics," in *Robotics: Science and Systems (RSS)*, 2017, dataset:[berkeleyautomation.github.io/dex-net/](https://github.com/berkeleyautomation.github.io/dex-net/).
- [5] D. Kalashnikov, A. Irpan, P. Pastor, J. Ibarz, A. Herzog, E. Jang, D. Quillen, E. Holly, M. Kalakrishnan, V. Vanhoucke, and S. Levine, "QT-Opt: Scalable Deep Reinforcement Learning for Vision-Based Robotic Manipulation," *ArXiv e-prints*, June 2018. [Online]. Available: <https://arxiv.org/abs/1806.10293>
- [6] B. Zoph, V. Vasudevan, J. Shlens, and Q. V. Le, "Learning transferable architectures for scalable image recognition," *Computer Vision and Pattern Recognition (CVPR)*, 2018. [Online]. Available: <http://arxiv.org/abs/1707.07012>
- [7] I. Lenz, H. Lee, and A. Saxena, "Deep learning for detecting robotic grasps," *The International Journal of Robotics Research*, vol. 34, no. 4-5, pp. 705–724, 2015, dataset:<http://pr.cs.cornell.edu/grasping/rect>. [Online]. Available: <https://doi.org/10.1177/0278364914549607>
- [8] A. Depierre, E. Dellandrea, and L. Chen, "Jacquard: A Large Scale Dataset for Robotic Grasp Detection," *ArXiv e-prints*, Mar. 2018. [Online]. Available: <http://arxiv.org/abs/1803.11469>
- [9] K.-T. Yu, M. Bauza, N. Fazeli, and A. Rodriguez, "More than a million ways to be pushed: a high-fidelity experimental dataset of planar pushing," in *Intelligent Robots and Systems (IROS), 2016 IEEE/RSJ International Conference on*. IEEE, 2016, pp. 30–37. [Online]. Available: <http://arxiv.org/abs/1604.04038>
- [10] Y. Zhu, Z. Wang, J. Merel, A. A. Rusu, T. Erez, S. Cabi, S. Tunyasuvunakool, J. Kramr, R. Hadsell, N. de Freitas, and N. Heess, "Reinforcement and imitation learning for diverse visuomotor skills," in *Robotics: Science and Systems XIV*, vol. 14, 2018. [Online]. Available: <http://arxiv.org/abs/1802.09564>
- [11] S. Levine, C. Finn, T. Darrell, and P. Abbeel, "End-to-end training of deep visuomotor policies," *Journal of Machine Learning Research*, vol. 17, no. 39, pp. 1–40, 2016.
- [12] L. Pinto and A. Gupta, "Supersizing self-supervision: Learning to grasp from 50k tries and 700 robot hours," in *2016 IEEE International Conference on Robotics and Automation (ICRA)*, 2016, pp. 3406–3413. [Online]. Available: <http://arxiv.org/abs/1509.06825>
- [13] E. Jang, S. Vijayanarasimhan, P. Pastor, J. Ibarz, and S. Levine, "End-to-End Learning of Semantic Grasping," *ArXiv e-prints*, July 2017. [Online]. Available: <http://arxiv.org/abs/1707.01932>
- [14] P. Agrawal, A. V. Nair, P. Abbeel, J. Malik, and S. Levine, "Learning to poke by poking: Experiential learning of intuitive physics," *neural information processing systems*, vol. abs/1606.07419, pp. 5074–5082, 2016. [Online]. Available: <http://arxiv.org/abs/1606.07419>
- [15] J. Redmon and A. Angelova, "Real-time grasp detection using convolutional neural networks," *CoRR*, vol. abs/1412.3128, 2014. [Online]. Available: <http://arxiv.org/abs/1412.3128>
- [16] I. Mordatch, N. Mishra, C. Eppner, and P. Abbeel, "Combining model-based policy search with online model learning for control of physical humanoids," in *ICRA 2016, Stockholm, Sweden, May 16-21, 2016*, 2016, pp. 242–248. [Online]. Available: <http://dx.doi.org/10.1109/ICRA.2016.7487140>
- [17] D. Xu, S. Nair, Y. Zhu, J. Gao, A. Garg, L. Fei-Fei, and S. Savarese, "Neural Task Programming: Learning to Generalize Across Hierarchical Tasks," *Robotics and Automation (ICRA), 2017 IEEE International Conference on*, Oct. 2018. [Online]. Available: <https://arxiv.org/abs/1710.01813>
- [18] D. Morrison, P. Corke, and J. Leitner, "Closing the Loop for Robotic Grasping: A Real-time, Generative Grasp Synthesis Approach," *ArXiv e-prints*, Apr. 2018.
- [19] E. Jang, S. Vijayanarasimhan, P. Pastor, J. Ibarz, and S. Levine, "End-to-end learning of semantic grasping," in *Proceedings of the 1st Annual Conference on Robot Learning*, ser. Proceedings of Machine Learning Research, S. Levine, V. Vanhoucke, and K. Goldberg, Eds., vol. 78. PMLR, 13–15 Nov 2017, pp. 119–132. [Online]. Available: <http://proceedings.mlr.press/v78/jang17a.html>
- [20] T. Elsken, J. Hendrik Metzen, and F. Hutter, "Neural Architecture Search: A Survey," *ArXiv e-prints*, Aug. 2018. [Online]. Available: <http://arxiv.org/abs/1808.05377>
- [21] C. Paxton, V. Raman, G. D. Hager, and M. Kobilarov, "Combining neural networks and tree search for task and motion planning in challenging environments," in *2017 IEEE/RSJ International Conference on Intelligent Robots and Systems (IROS)*, 2017, pp. 6059–6066. [Online]. Available: <http://arxiv.org/abs/1703.07887>
- [22] C. Paxton, F. Jonathan, A. Hundt, B. Mutlu, and G. D. Hager, "Evaluating methods for end-user creation of robot task plans," *Intelligent Robots and Systems (IROS), 2018 IEEE International Conference on*, 2018, to appear.
- [23] Y. Xiang, T. Schmidt, V. Narayanan, and D. Fox, "Posecnn: A convolutional neural network for 6d object pose estimation in cluttered scenes," in *Robotics: Science and Systems (RSS)*, vol. 14, 2018. [Online]. Available: <https://arxiv.org/abs/1711.00199>
- [24] C. Li, J. Bai, and G. D. Hager, "A Unified Framework for Multi-View Multi-Class Object Pose Estimation," *ArXiv e-prints*, Mar. 2018.
- [25] A. Byravan and D. Fox, "Se3-nets: Learning rigid body motion using deep neural networks," *arXiv preprint arXiv:1606.02378*, 2016.
- [26] F. Chollet et al., "Keras," <https://keras.io>, 2015.
- [27] M. Abadi, A. Agarwal, P. Barham, E. Brevdo, Z. Chen, C. Citro, G. S. Corrado, A. Davis, J. Dean, M. Devin, S. Ghemawat, I. Goodfellow, A. Harp, G. Irving, M. Isard, Y. Jia, R. Jozefowicz, L. Kaiser, M. Kudlur, J. Levenberg, D. Mané, R. Monga, S. Moore, D. Murray, C. Olah, M. Schuster, J. Shlens, B. Steiner, I. Sutskever, K. Talwar, P. Tucker, V. Vanhoucke, V. Vasudevan, F. Viégas, O. Vinyals, P. Warden, M. Wattenberg, M. Wicke, Y. Yu, and X. Zheng, "TensorFlow: Large-scale machine learning on heterogeneous systems," 2015, software available from tensorflow.org. [Online]. Available: <https://www.tensorflow.org/>
- [28] T. G. authors, "GPYOpt: A bayesian optimization framework in python," <http://github.com/SheffieldML/GPYOpt>, 2016.
- [29] K. Simonyan and A. Zisserman, "Very deep convolutional networks for large-scale image recognition," *International Conference on Learning Representations*, 2015. [Online]. Available: <http://arxiv.org/abs/1409.1556>
- [30] G. Huang, Z. Liu, L. van der Maaten, and K. Q. Weinberger, "Densely Connected Convolutional Networks," *ArXiv e-prints*, Aug. 2016.
- [31] K. He, X. Zhang, S. Ren, and J. Sun, "Identity mappings in deep residual networks," *europaean conference on computer vision*, pp. 630–645, 2016. [Online]. Available: <http://arxiv.org/abs/1603.05027>
- [32] K. He, X. Zhang, S. Ren, and J. Sun, "Deep residual learning for image recognition," in *2016 IEEE Conference on Computer Vision and Pattern Recognition (CVPR)*, 2016, pp. 770–778. [Online]. Available: <http://arxiv.org/abs/1512.03385>
- [33] C. Szegedy, S. Ioffe, V. Vanhoucke, and A. A. Alemi, "Inception-v4, inception-resnet and the impact of residual connections on learning," *national conference on artificial intelligence*, pp. 4278–4284, Feb. 2016.
- [34] R. Liu, J. Lehman, P. Molino, F. Petroski Such, E. Frank, A. Sergeev, and J. Yosinski, "An Intriguing Failing of Convolutional Neural Networks and the CoordConv Solution," *ArXiv e-prints*, July 2018. [Online]. Available: <https://arxiv.org/abs/1807.03247>
- [35] A. Krizhevsky. (2009) Learning multiple layers of features from tiny images. [Online]. Available: <https://www.cs.toronto.edu/~kriz/learning-features-2009-TR.pdf>
- [36] H. Xiao, K. Rasul, and R. Vollgraf, "Fashion-mnist: a novel image dataset for benchmarking machine learning algorithms," *ArXiv e-prints*, 2017. [Online]. Available: <http://arxiv.org/abs/1707.07012>